Control of a Two Dimensional Target Seeking Rocket

Jacob Koos*, Boluwatife Olabiran*, Muhammad Saud Ul Hassan* and Brian Van Stratum*

***Abstract*— We propose to control the heading angle of a rocket by actuating control surfaces. We will develop equations of motion of the rocket as well as model the internal electro-mechanical dynamics . Various non-linearities will be addressed, and the time domain response of the system will be compared to desired performance.**

I. INTRODUCTION

A rocket flying through the atmosphere heading for a target presents an interesting and practical challenge for closed loop feedback control. In fact, the development and application of classical control theory is intimately tied to the development of rocket guidance systems by way of the infamous V-2 rocket and Wernher von Braun [1]. This control problem has multiple opportunities for exploring both linear and non-linear effects.

II. METHODS

We propose to simulate the path of a self guiding rocket with the intent of hitting a desired target. The rocket will be launched with initial input of desired angle of attack. Once launched the rocket will then begin to adjust the heading angle in its pursuit of the position of the target.

A. Equations of Motion

Reliable models have been proposed for representing a rocket for the purpose of control. These models are reproduced in [3]. Compared to Lastimo et al, we propose a simplified planar rocket model in two dimensions given by the following equations of motion:

$$\sum F_x = m\ddot{x} = Tcos(\theta) - b_1\dot{x}^2 \tag{1}$$

$$\sum F_y = m\ddot{y} = Tsin(\theta) - b_2\dot{y}^2 \tag{2}$$

$$\sum M = I\alpha = I\ddot{\theta} = k\psi \tag{3}$$

$$T = \dot{m}\,u \tag{4}$$

Where T in equations 1, 2 and 4 is the magnitude of the thrust of the rocket. The variable k in 3 is the constant of proportionality between the control torque and the angle of attack (ψ). This torque is induced by the angle of attack of the control surface at the back of the rocket. The b_1 and b_2 terms in 1 and 2 are to account for aerodynamic drag, and u and $\dot{m}$ are the exhaust velocity and mass flow rate of jet fuel, respectively. These equations of motion have been developed into both a state-space formulation as well as a Simulink model for the purpose of testing controllers.

The equations 1,2 and 3 can be rearranged into the following state space formulation in order to be simulated using ODE45. Note that since these are non-linear equations, the format does not conform to the standard state-space formulation of $\dot{z} = Az + B$. *See Appendix A of the midterm update report for a full derivation and Appendix B for the ODE45 simulation code.*

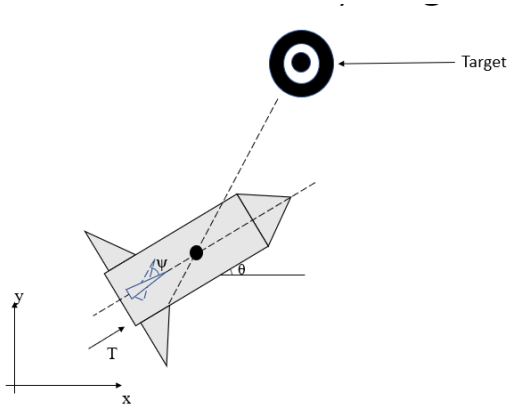

Fig. 1. Free Body Diagram for Rocket Plant

$$\vec{z} = \begin{pmatrix} x \\ \dot{x} \\ y \\ \dot{y} \\ \theta \\ \dot{\theta} \end{pmatrix} \tag{5}$$

$$\dot{\vec{z}} = \begin{pmatrix} z_2 \\ \frac{u}{m_i}\,\dot{m}\,cos(z_5) - \frac{b_1}{m_i}\,z_2^2 \\ z_4 \\ \frac{u}{m_i}\,\dot{m}\,sin(z_5) - \frac{b_1}{m_i}\,z_2^2 \\ z_6 \\ \frac{k}{I}\,\psi \end{pmatrix} \tag{6}$$

Where m_i is the rocket's initial mass.

B. Rocket Plant Simulation Output

The state space model in equation 6 was run three times with three different steady torques applied by the control surfaces at the rear of the rocket. Figure 2 shows the trajectories for these torques. Note that the rocket is becoming unstable at approximately 100 m downrange. This is approximately half a second after launch. This time-frame is significant for the controller design. These trajectories are animated in the provided video files attached along with this report.

C. DC Motor Model

Further, we have modeled the electro-mechanical dynamics of the rocket's control surface. The control surface's angle

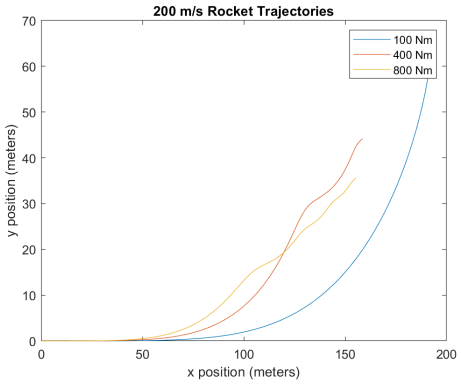

Fig. 2. Three Rocket Trajectories Applying Constant Torque

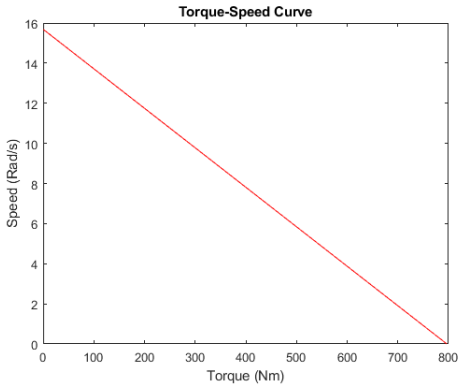

Fig. 3. Torqe Speed Plot

of attack, $\psi(t)$, can be modeled as the transfer function $G_m(s)$ relating an applied voltage, $E_a(s)$, to the output, the angle of attack, $\Psi(s)$. We have developed the equations of this model. It is expected to be similar to equation 7 from [2].

$$G_m(s) = \frac{\Psi_m(s)}{E_a(s)} = \frac{K}{s(s+a)} \tag{7}$$

To come up with the transfer function for the DC motor we begin with an equation proportionally relating the current carrying armature's voltage to speed:

$$v_b(t) = K_b(\frac{d\theta_m(t)}{dt}) \tag{8}$$

Where $v_b(t)$ is equal to the back emf and K_b is the back emf constant. By taking the Laplace transform of 8 we get

$$V_b(s) = K_b s\theta_m(s) \tag{9}$$

We can then write the loop equation for the Laplace transformed armature circuit. This allows us to derive a relationship between the armature current, $I_a(s)$, the applied armature voltage, $E_a(s)$, and the back emf,$V_b(s)$:

$$R_a I_a(s) + L_a s I_a(s) + V_b(s) = E_a(s) \tag{10}$$

We also know that the torque developed by the motor, $T_m(s)$, is proportional to the armature current:

$$T_m(s) = K_t I_a(s) \tag{11}$$

Where K_t is the motor torque constant. Now, we find the torque developed by the motor in terms of $\theta_m(s)$. With J_m as the inertia at the armature and D_m as the viscous damping at the armature, we can write

$$T_m(s) = (J_m s^2 + D_m s + K_s)\theta_m(s) = k\Psi(s) \tag{12}$$

Where $T_m(s)$ in this equation is equivalent to the typical loading on a motor. These derivations can be found in Nise[2], but must be modified to account for the interaction of the control surface and the electromechanics of the motor. Constants in equations 8 through 12 are calculated from a torque vs. motor-speed curve, like the one we have produced for our motor in figure 3.

The equations 8 through 12 have been modeled in Simulink. Figure 4 shows the motor's transient performance to a voltage step input. Note that the aileron motor is able to generate 300 $N\,m$ of Torque in about half a second. Given the speeds that we are considering, this should provide enough control effort to develop a controller.

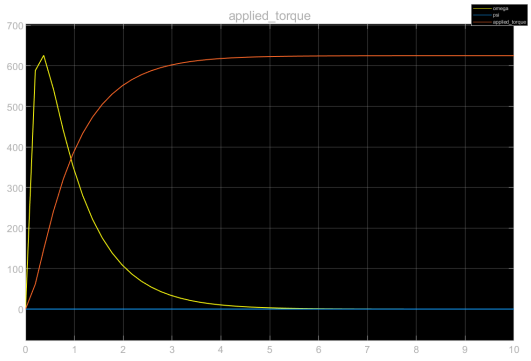

Fig. 4. Aeleron Motor Performance

D. Control

Our control strategy is to sense the heading angle of the rocket and use it to generate an error signal relative to a constant command. The error is used to drive a DC motor that turns the control surface. This strategy is illustrated in Fig 5.

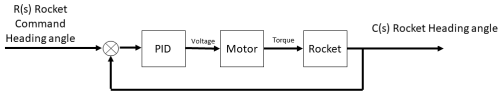

Fig. 5. Block Diagram of Control Strategy

Solving Eq. 3,10 and 12 simultaneously gives

$$\frac{\Theta_h(s)}{E_a(s)} = \frac{K_s K_t}{Is^2(J_m R_a s^2 + (D_m R_a + K_b k_t)s + K_s R_a)} \tag{13}$$

These equations have the root locus shown in Fig. 6. This root locus has two branches that are unstable for every gain. Thus we need a controller.

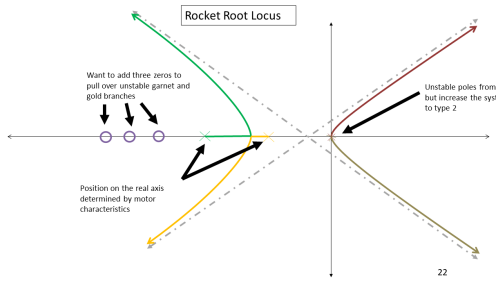

Fig. 6. Rocket's Uncontrolled Root Locus

Adding a PID controller with poles located as shown in purple in Fig. 7 pulls the unstable garnet and gold poles over into the stable left half plane for gains in a certain range.

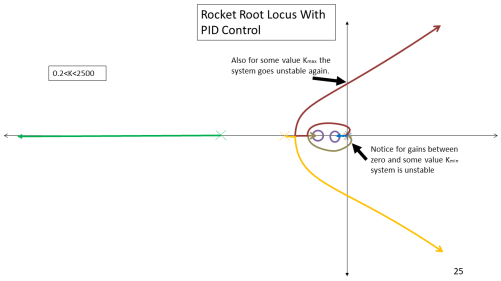

Fig. 7. Rocket's Motor and PID Controller Root Locus

A gain was chosen that gives a slight overshoot and a rise time of about half-a-second. Fig. 8 shows the simulated angle response to a step input of 1 Rad. Fig. 9 shows the applied voltage and current at the motor during such a step transient.

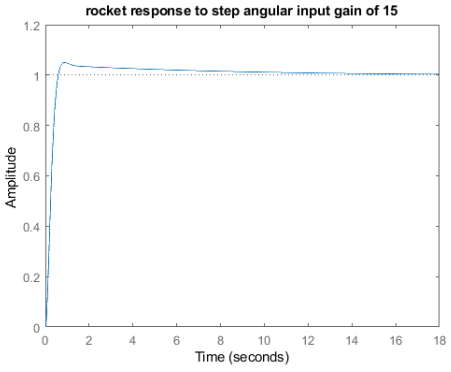

Fig. 8. Rocket's Controlled Response to a Step angular Input of One Radian

Finally, a simulated rocket Cartesian trajectory is shown in Fig. 10. In this figure, we see the rocket's heading angle stabilize to the commanded 45^o in the settling time that we designed for.

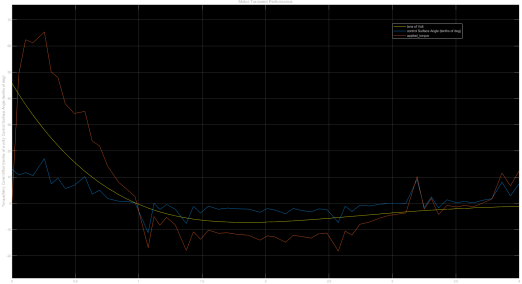

Fig. 9. Motor's Transient Response to 45^o Step Input

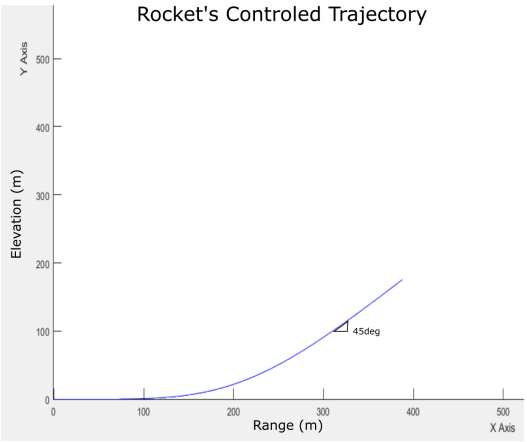

Fig. 10. Rocket's Controlled Trajectory Response to 45^oStep Input

E. Non-Linearity

The plant model has various non-linear effects that arise from trigonometric and algebraic functions and the non-linear nature of drag. The non-linearities that we will be addressing include the drag on the aileron, filtering out non-linear noise that we will be injecting into the system, motor saturation, and non-linearities in the plant. We propose to linearize these effects at our operating points. Viable options include small angle assumptions and Taylor series expansions near the operating point of the rocket.

1) Aileron Drag: The non-linear aerodynamic drag force (F_d) acting on the control surface produces a torque in the motor (τ_d) that opposes the control torque. The effect the aerodynamic drag has on the system's dynamics must, therefore, be adequately accounted for in the controller's design.

Assuming the control surface to be a thin, solid, plate of length l and height h, we can arrive at the following equation for the aerodynamic drag:

$$F_d(t) = \frac{1}{2}\,\rho\, v(t)^2\,[\,l\,h\,sin\psi(t)\,]\,C_D \tag{14}$$

Where ρ is the density of air, which we have assumed to be constant over the flight path, v is the rocket's velocity, and C_D is the drag coefficient, which has experimentally been established by previous studies to be around 0.005 for a thin plate moving through a fluid at high speeds.

Substituting the constants in Eq. 14 gives

$$F_d = (\,0.003115\, l\, h\,)\, sin\psi(t)\; v(t)^2 \tag{15}$$

One can find the torque that this aerodynamic drag would generate as

$$T_d = \frac{l}{2}\, F_d = (\,0.00156\, l^2\, h\,)\, sin\psi(t)\; v(t)^2 \tag{16}$$

For the sake of simplicity, T_d can be linearized about the average velocity, v_{avg}. The linearization is particularly valid for small values of ψ, as can be seen in Fig. 11

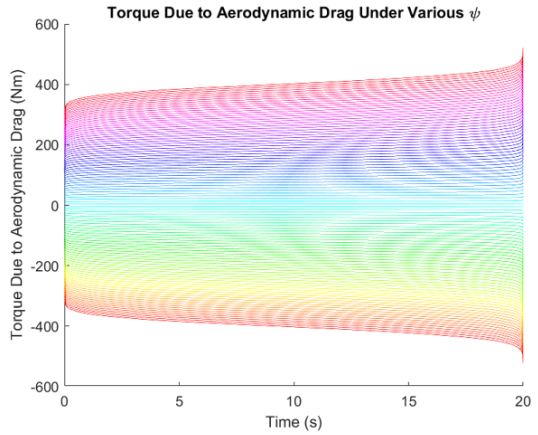

Fig. 11. Torque Due to Aerodynamic Drag Under Different Values of Aileron Angle, ψ

Assuming $-45^o < \psi < 45^o$, Eq. 16 can be linearized to

$$T_d = (\,0.00156\, l^2\, h\, v_{avg}^2\,)\, \psi(t) = 570\; \psi(t) \tag{17}$$

2) Non-linear Noise: For this aspect of non-linearity, we propose to add a non-linear disturbance to our system and filter it out through a low pass filter. The transfer function for the low-pass filter is given in Eq. 18.

$$\frac{1/T}{s + (1/T)} \tag{18}$$

Where T is the filter time constant. First, we set out to create a simplified version of the low-pass filter to test how it would attenuate the noise. This simplified block diagram can be seen in Fig 12.

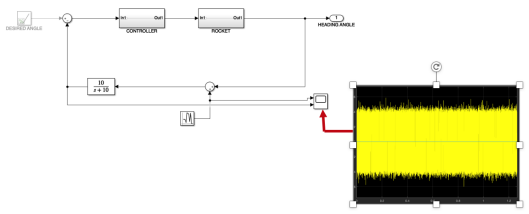

Fig. 12. Simplified Block Diagram of Low Pass filter

After establishing that the designed low-pass filter can successfully attenuate the injected noise signal, we proceeded to implement it into the system. Within the system, the signal was staying around $7.37e^3 rad/s$, due to this we decided to set the cutoff frequency to two decades later, at around $7.37e^5 rad/s$. We arrived at this cutoff frequency because we did not want to attenuate signals close to the system's own signals.

With the cutoff frequency set, a range was created for the noise disturbance between $10^6 - 10^7 rad/s$. Eq. 19 shows the new transfer function derived with the set cutoff frequency. The Bode plot for this transfer function can be seen as well in Fig. 13, Where the red line represents the cutoff frequency and the green line is the frequency of the noise signal.

$$\frac{7.37 \times 10^5}{s + (7.37 \times 10^5)} \tag{19}$$

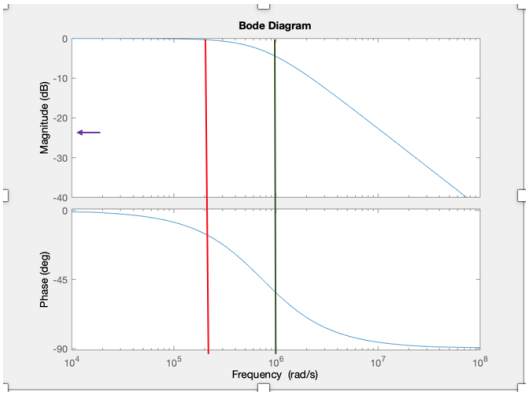

Fig. 13. Bode Plot of New Low Pass Filter Transfer Function

3) Motor Saturation: Since the non-linear characteristics of the control surface have been linearized, it is also necessary to model the effect of control surface saturation. This accounts for the fact that a control surface does not have an infinite torque response. Fig. 14 shows the control surface torque model responding to a ramp angular input from $-90°$ to $90°$ shown by the yellow trace. The blue trace shows the torque applied by the control surface to the rocket. It is limited to a maximum value. This behaviour would be somewhat accounted for by the fact that the equations 10 and 12 do accurately model the stall torque, but it provides an added layer of realistic behavior.

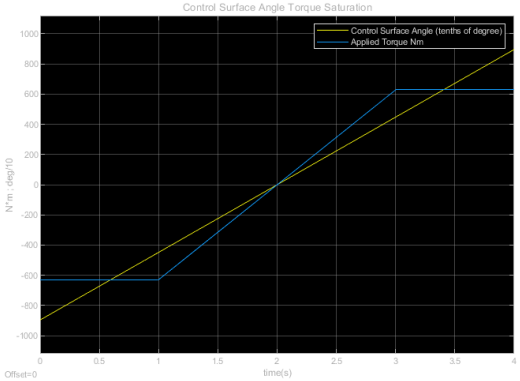

Fig. 14. Torque Response Saturation at 45^o

4) Plant Non-Linearity's: As can be seen from the model equations of motion described in equations 1, 2 3, the motion of the plant in the x and y directions is made up of trigonometric and square functions. The presence of these trigonometric and square functions makes the motion of the plant a non-linear one. To address this, the equations of motion were developed into a state-space model. This is because state-space models can work well and directly with non-linear systems.

III. EVALUATING RESULTS

We proposed that the performance of the rocket simply be categorized based on whether or not the rocket was able to hit the target given various rocket target initial conditions. We have demonstrated that our controller has an acceptable response. The rocket is able to achieve a stable heading in about 1 second at our speeds that refers to a downrange distance of about 200 meters. We have designed our controller to give a faster rise time and we accept a small overshoot for that. This implies that targets that are not at least 300 meters or so downrange are not possible to hit. For typical rocket speeds this is acceptable.

REFERENCES

[1] M.J. Neufeld, The Rocket and the Reich: Peenemunde and the coming of the Ballistic Missile Era. New York: The Free Press.

[2] N.S. Nise, Control Systems Engineering 6th Edition pp. 78.

[3] D. Lastomo, Setiadi,and Djalal "Optimization pitch angle controller of rocket system using improved differential evolution algorithm" International Journal of Advances in Intelligent Informatics Vol 3, No. 1, March 2017 PP. 27-34.